STRUCTURAL BIOLOGY

ISSN: 2059-7983
journals.iucr.org/d

Membrane-protein crystals for neutron diffraction

Thomas Lykke-Møller Sørensen, Samuel John Hjorth-Jensen, Esko Oksanen, Jacob Lauwring Andersen, Claus Olesen, Jesper Vuust Møller and Poul Nissen

Acta Cryst. (2018). D**74**, 1208–1218

STRUCTURAL BIOLOGY
ISSN 2059-7983

Membrane-protein crystals for neutron diffraction

Thomas Lykke-Møller Sørensen,[a]* Samuel John Hjorth-Jensen,[a] Esko Oksanen,[b,c] Jacob Lauwring Andersen,[d] Claus Olesen,[d] Jesper Vuust Møller[d] and Poul Nissen[a]*

[a]Department of Molecular Biology and Genetics – DANDRITE, Aarhus University, Gustav Wieds Vej 10, DK-8000 Aarhus C, Denmark, [b]European Spallation Source ERIC, PO Box 176, 22100 Lund, Sweden, [c]Department of Biochemistry and Structural Biology, Lund University, PO Box 124, 22100 Lund, Sweden, and [d]Department of Biomedicine, Aarhus University, Ole Worn Alle 3, DK-8000 Aarhus C, Denmark. *Correspondence e-mail: tlms@mbg.au.dk, pn@mbg.au.dk

Received 11 June 2018
Accepted 5 September 2018

Edited by V. T. Forsyth, Institut Laue-Langevin, France, and Keele University, UK

Keywords: neutron macromolecular crystallography; membrane-protein crystallization; structural biology; SERCA1.

Supporting information: this article has supporting information at journals.iucr.org/d

Neutron macromolecular crystallography (NMX) has the potential to provide the experimental input to address unresolved aspects of transport mechanisms and protonation in membrane proteins. However, despite this clear scientific motivation, the practical challenges of obtaining crystals that are large enough to make NMX feasible have so far been prohibitive. Here, the potential impact on feasibility of a more powerful neutron source is reviewed and a strategy for obtaining larger crystals is formulated, exemplified by the calcium-transporting ATPase SERCA1. The challenges encountered at the various steps in the process from crystal nucleation and growth to crystal mounting are explored, and it is demonstrated that NMX-compatible membrane-protein crystals can indeed be obtained.

1. Introduction

Neutron macromolecular crystallography (NMX) has so far featured on the fringe of structural biology as a technique with the potential to identify the individual protons integral to catalytic processes and reveal how H atoms shape interaction sites (Blakeley *et al.*, 2015). Considering how unassuming the H atom is, it has a huge influence on the processes that constitute life. Understanding the protonation state of amino-acid residues and the transfer of protons between them, or to cofactors and substrates, is key to understanding catalytic processes in biology (Oksanen *et al.*, 2017). Determining H-atom positions in enzyme active sites or at drug-binding sites may enhance our prediction power in a structure-based drug-design process (Weber *et al.*, 2013; Gerlits *et al.*, 2017).

Through NMX, we can gain a better understanding of membrane-protein mechanisms that we currently only assume from modelling. A range of membrane proteins are dedicated to moving protons up or down their electrochemical gradients. Prime examples are the various complexes in photosynthesis and oxidative phosphorylation that generate the proton gradient utilized by F_1F_o-ATPase to synthesize ATP (Walker, 2013), and the P-type ATPases such as the fungal H^+-ATPase (Buch-Pedersen *et al.*, 2009) and mammalian H^+/K^+-ATPases (Sakai *et al.*, 2016) that transport protons across the membrane in an ATP-consuming process. Finally, a whole host of secondary transporters tap into the energy stored in the proton gradients to transport essential building blocks such as amino acids and sugars across the membrane (Newstead, 2015). Common to all these processes is that we only have circumstantial structural evidence for the actual processes, as the protons elude us in the electron-density maps obtained by X-ray macromolecular crystallography (MX).

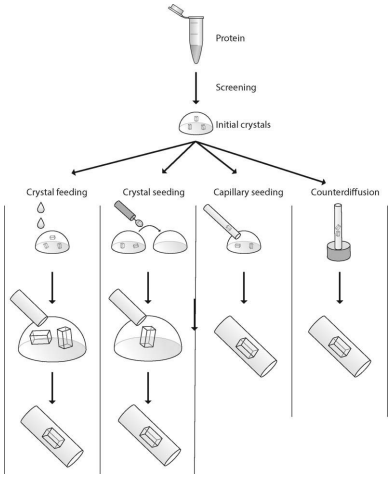

However, the current price that must be paid for the insight that NMX provides is high and can only be met by producing large, well diffracting crystals. Since the diffracted intensity is directly proportional to that of the incident beam (O'Dell *et al.*, 2016), these large crystals are required because of the inherently lower neutron flux at a neutron-source instrument ($<10^8$ neutrons per mm^2 per second) compared with the photon flux that the MX community is used to at standard synchrotron beamlines ($>10^{12}$ photons per 100 µm^2 per second and generally stronger scattering cross-sections) (Blakeley *et al.*, 2008). If we further consider the recent trends in MX towards smaller crystals, microfocus X-ray beams, *in situ* studies and serial data collection (Jaeger *et al.*, 2016), the price of NMX appears to have increased even further over current state-of-the-art X-ray crystallography.

At the time of writing, the Protein Data Bank (PDB) contains 142 protein structures of 52 different proteins obtained by NMX, and so far there are no membrane-protein structures on the list. This may be about to change. The European Spallation Source (ESS), which is currently under construction in Lund, Sweden, will house a new NMX instrument connected to what will become the world's most powerful neutron source (https://europeanspallationsource.se/instruments/nmx). In ideal cases, the NMX instrument planned for the ESS is expected to deliver enough neutrons to make it possible to collect a diffraction data set to 2 Å resolution with >90% completeness from a crystal of 0.1 mm^3 volume and unit-cell dimensions of up to 150 Å in a day. For smaller crystals or larger unit-cell dimensions, data collection should remain possible, although requiring data-collection times of the order of days, but will certainly open the field of opportunity to include membrane-protein crystals.

More than a decade ago, we reviewed the state of membrane-protein crystallography at the time (Sørensen *et al.*, 2006). The various crystallization techniques used in MX have been extensively reviewed elsewhere (McPherson, 2017; Gavira, 2016) and here we will briefly comment on key approaches in light of the specific challenges of NMX and give examples of how we have used these approaches to obtain large crystals of the calcium-transporting ATPase SERCA1.

2. Ideal membrane-protein targets

Membrane proteins are challenging structural biology. The ratio of membrane-protein to soluble-protein structures amongst the more than 140 000 structures in the PDB in 2018 is roughly 1:60. This clearly illustrates the added complexity of solving membrane-protein structures, where the path from target selection to structure is often akin to a winding and treacherous mountain pass. Several elements inherent to membrane proteins generally contribute to the difficulties: low levels of expression, the additional requirement for detergents, and poor protein stability when solubilized. These three factors ultimately mean less protein for crystallization. Fortunately, automation and denser crystallization formats have enabled the reduction of crystallization volumes for a typical vapour-diffusion experiment to 100–200 nl per condition. Hence, with only 10 µl of a precious membrane-protein sample, a 96-well crystallization-plates-worth of crystallization experiments can be set up (Kang *et al.*, 2013; Moraes *et al.*, 2014).

To provide new detailed information about protonation, the resolution of an NMX structure should ideally be better than 2.5 Å. Of the membrane-protein structures in the PDB, only about 40% are at a resolution of 2.5 Å or better, compared with about 75% for the entire PDB. The numbers are skewed by the high impact of new membrane-protein structures, making lower resolution structures more readily publishable, but it also reflects the fact that membrane-protein crystals typically contain a larger fraction of solvent, which may also include disordered lipids and detergents.

Several membrane-protein structures have been determined at high resolution from fairly large crystals and with reasonable unit-cell parameters, such as the photosynthetic reaction centre, bacteriorhodopsin, many aquaporins and the ammonia transporter. Supplementary Table S1 lists examples of membrane proteins with reported crystal forms that it would be feasible to pursue for NMX based on their unit-cell parameters, crystal size potential and the resolution obtained in the studies referenced.

2.1. SERCA as an NMX candidate

The calcium-transporting ATPase from the sarco-endoplasmic reticulum (SERCA) is a difficult but conceivable target for an NMX experiment, and there are key questions concerning the protonation and hydrogen-bonding patterns of side chains at the calcium-binding sites in the membrane, the counter-transport of protons and the catalytic properties of the phosphorylation/dephosphorylation site, where NMX could provide important information on how SERCA and P-type ATPases in general work, are affected by disease-causing mutations and are regulated by inhibitors, lipids and other cofactors.

SERCA transports calcium and protons in opposite directions across the endoplasmic reticulum membrane, utilizing energy derived from ATP hydrolysis to fuel the process. The general physiological role of SERCA is to perform (re)uptake of cytoplasmic calcium to internal stores of the ER, and specifically to terminate calcium-induced muscle contraction in myocytes (Møller *et al.*, 2010). As illustrated in the simplified reaction scheme for SERCA in Fig. 1, once two calcium ions have been released inside the ER, two to three protons bind to residues in the transmembrane region and are counter-transported as part of the process to revert the orientation of the membrane-located ion-binding site. The protons are likely to reduce excess negative charge at the binding site, thereby lowering the energy barrier for the conformational changes that make up the reorientation of the binding sites. Protonation remains undetermined at the resolution of the MX structures obtained so far. Another puzzle is the route that the protons follow through SERCA as they are released towards the cytoplasm. Mutational (Sørensen & Andersen, 2000) and structural (Bublitz *et al.*, 2013) analyses have identified a

potential hydrated pathway through the C-terminal transmembrane region of the protein. Recent structural analysis and MD simulations (Espinoza-Fonseca, 2017) have identified additional hydrated pathways through the transmembrane region of SERCA which may form a pore that allows bidirectional proton transport during enzyme turnover. In conclusion, the determination of an NMX structure of SERCA would help us to address the potential path(s) and the underlying transport mechanism unambiguously.

The PDB currently contains 72 structures of SERCA captured in various intermediate conformations in the presence of a range of different inhibitors. A quarter of the deposited structures are at 2.5 Å resolution or better, and Supplementary Table S2 summarizes SERCA crystal forms with unit-cell parameters amenable to NMX data collection and structure solution. Not all crystal forms will work well with neutrons, one example being PDB entry 2c8l and many related entries representing a proton-occluded E2 state crystallized in a $P4_12_12$ crystal form with a c axis of almost 600 Å, *i.e.* well outside the range that can be resolved on a neutron detector (Toyoshima & Nomura, 2002; Jensen *et al.*, 2006). Some structures are similar but are solved in different crystal forms. An example is found in PDB entries 3n5k and 1xp5, both of which are structures of SERCA captured in the dephosphorylating proton-occluded E2-P_i-like intermediate with aluminium fluoride and the inhibitor thapsigargin (Bublitz *et al.*, 2013; Olesen *et al.*, 2004). The form reported in PDB entry 1xp5 has not been pushed to higher resolution to date, but this would seem to be possible as it has been achieved for the aforementioned PDB entry 3n5k and also for a $P2_1$ form (PDB entry 1wpg; Toyoshima *et al.*, 2004), both of which displayed a related packing of molecules. Another possible case for SERCA NMX studies relates to the calcium-occluded E1-ATP forms obtained with, for example, AMPPCP, ADP:AlF_4^- and AMPPNP analogues (Sørensen *et al.*, 2004; Toyoshima & Mizutani, 2004; Jensen *et al.*, 2006; Olesen *et al.*, 2007). The unit-cell dimensions are manageable (Table 2) and diffraction has currently reached 2.4 Å resolution in published structures.

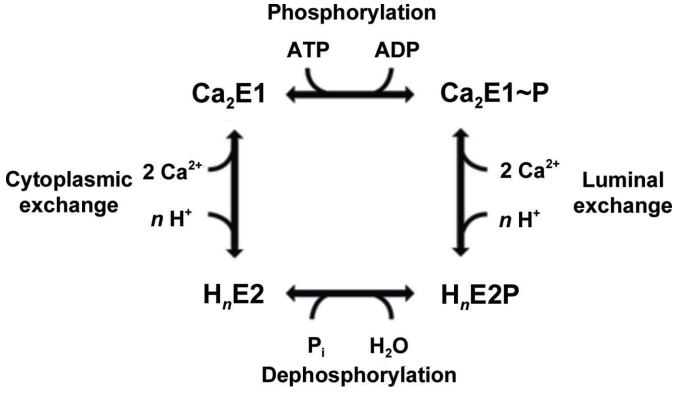

Figure 1
Schematic of the SERCA enzyme cycle. The net outcome of each reaction cycle is the transport of two calcium ions from the cytoplasm to the lumen of the SER in exchange for n protons per ATP molecule hydrolysed.

3. SERCA crystallization

The crystal structures of SERCA deposited in the PDB have all been obtained by either vapour-diffusion or dialysis crystallization experiments. In our hands, vapour diffusion has been the most successful approach. Here, we have also pursued counter-diffusion crystallization to get a handle on the best way to obtain large well diffracting crystals suitable for NMX.

The protein used for our crystallization trials in this study was solubilized SERCA1 from native membranes isolated from homogenized muscle tissue by differential centrifugation (Møller *et al.*, 2002). This means that SERCA1 is in the presence of excess detergent and native lipids during crystallization. This approach has been termed the HiLiDe method (Gourdon *et al.*, 2011) and has proved to be very successful in our hands for obtaining the stable, solubilized membrane protein needed for crystallization trials. Batches of SERCA were solubilized from a common stock of native protein used for all crystallization trials. We see very limited batch-to-batch variation.

3.1. Vapour diffusion

Vapour diffusion is the method of choice for crystallization in MX. The principle is to mix protein and precipitant solutions in a droplet and equilibrate the mixture against a larger volume of precipitant solution within a confined space (McPherson, 2017). For SERCA, we typically set up 24-well hanging-drop crystallization experiments by hand (Bergfors, 2007), with each well sealed with immersion oil, which has a dramatic influence on crystal size and quality.

As previously reported (Sørensen *et al.*, 2006), we often see significant precipitation forming as the crystallization drops are set up. After initial matrix screening we therefore adopt a batch crystallization approach in which larger volumes of protein and precipitant solutions are mixed, incubated for ten minutes and centrifuged before being distributed as crystallization drops above solutions of increasing precipitant concentration. This approach significantly reduced the amount of nonproductive precipitation in our crystallization drops and tended to produce large single crystals (∼200 µm in the longest dimension) within three days (Fig. 2*a*).

To obtain larger crystals, more protein and hence larger crystallization drops were required. We first scaled the drop and reservoir volumes from 4 to 20 µl and from 0.4 to 1.0 ml respectively, and switched to a sitting-drop format to accommodate the increased drop size. However, the 20 µl drops behaved differently and we mostly saw dark-coloured precipitate and fewer, smaller crystals (Fig. 2*b*). This result highlights how strongly the dynamics within the crystallization drop are affected by changes in surface-area-to-volume ratios.

3.1.1. Crystal feeding. A potential solution is to allow nucleation/early-stage crystals to develop as normal within 4 µl drops followed by the addition of a larger volume of similar solution to the drop. With nucleation established, the added protein should contribute to the growth of existing crystals, with a lesser fraction being lost to nucleation

(Manzoni *et al.*, 2016). The results from experiments in which 4 µl drops were set up and left to nucleate for 24 h before 10 µl of batch solution of the same composition as the initial drops was added to each drop can be seen in Fig. 2(*c*). The results show that the behaviour change associated with increasing drop size is partially mitigated by this strategy. Crystal formation now follows that of the initial 4 µl scale experiment, and with larger crystals than the initial 4 µl drop and the 20 µl drop experiment alone. Interestingly, the single well within this plate that received an additional 10 µl of solubilized SERCA only exhibited delayed-onset crystal appearance and an extended growth phase, resulting in very large single crystals (Fig. 2*d*).

Decoupling small-volume nucleation from large-volume crystal development is a powerful technique for increasing crystal size. It also allows established crystallization protocols to be scaled up directly without significantly compromising crystal formation. Once nucleation has occurred, the mother liquor can be kept in the metastable phase by carefully selecting the composition and volume of any solution added. The rate of drop-volume change induced by vapour diffusion can also be carefully controlled by the volume and composition of the reservoir solution. The principle for controlling this phase–time pathway and the consequences for the

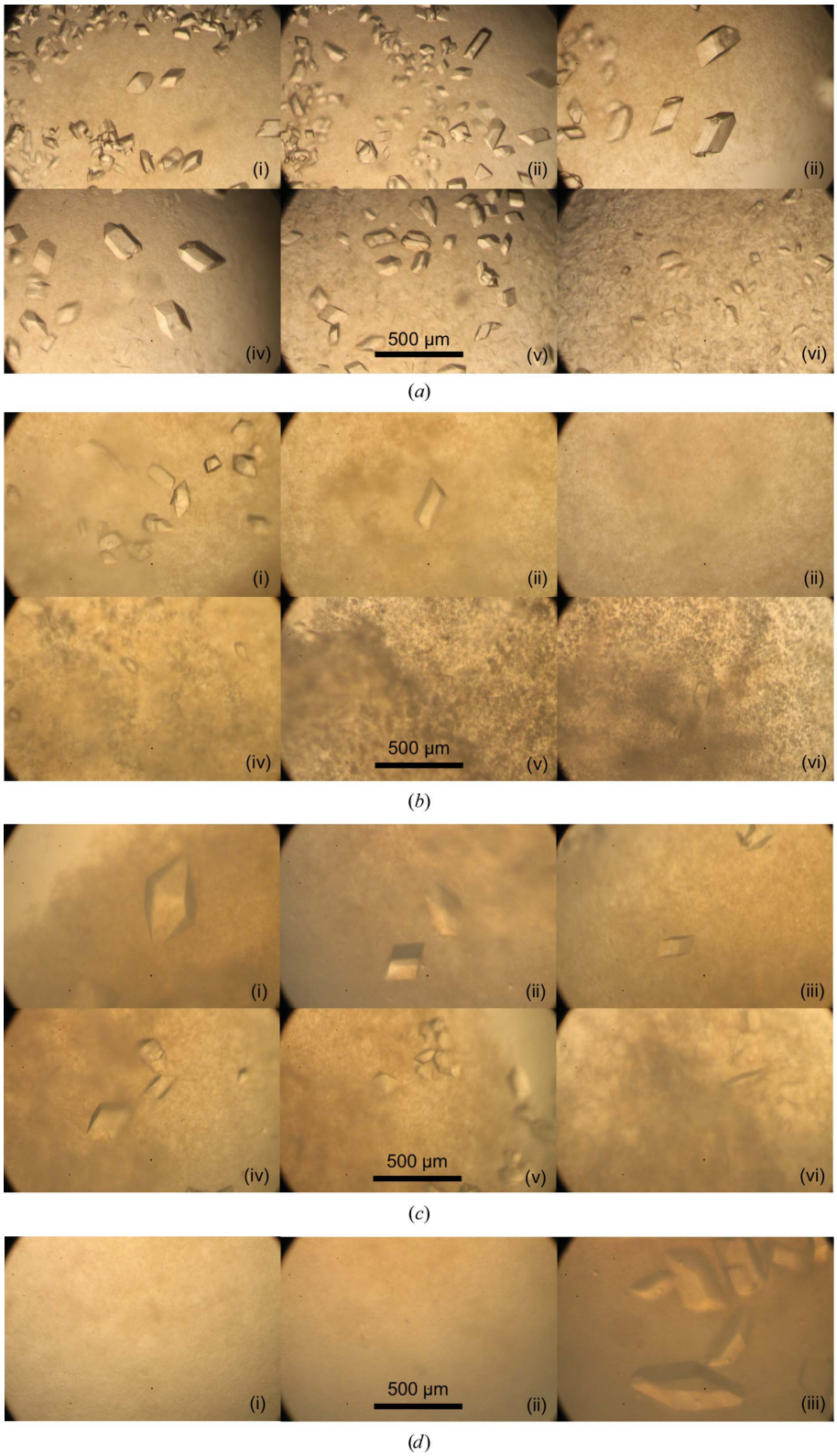

Figure 2
Effects of drop size on nucleation and crystal growth. (*a*) Images (i)–(vi) show identical 4 µl hanging drops suspended over 400 µl reservoir solution varying in glycerol content only (8–14%; 1.2% increments). The largest crystals appeared using glycerol concentrations in the reservoir in the range 10.4–11.6% (iii, iv). Images were taken ∼72 h after setup. (*b*) Images (i)–(vi) show identical 20 µl sitting drops with 1 ml reservoir solution varying in glycerol content only (8–14%; 1.2% increments). The largest crystals appeared using a glycerol concentration in the reservoir in the range 8.0–9.2% (i, ii). Of particular note are the comparatively large quantities of brown precipitate seen within the 20 µl drops, a behaviour that is antagonistic to crystal formation and growth. Images were taken ∼72 h after setup. (*c*) The drops in (i)–(vi) were allowed to nucleate for 24 h before a larger volume of protein/precipitate solution was added and proceeded through both a minimized, but nonzero, nucleation phase and an extended growth phase over the three-week period imaged. The crystal in (i) reached a final size that was greater than that in any other experiment so far, although the crystals in the remaining wells grew to a comparatively average size. (*d*) Finally, images (i)–(iii) track a single 4 µl drop (6% PEG 6000) suspended over a 400 µl reservoir solution consisting of 12% PEG 6000, 14% glycerol that was allowed to nucleate for 24 h before protein only was added. Although no crystals appeared 24 h after protein only was added (i) or after 5 days (ii), very large crystals appeared after three weeks (iii). These crystals approached 1 mm in the largest dimension, which was the result of a more optimal phase–time pathway.

crystallization of SERCA are summarized in Fig. 3. This strategy is essential for increasing the crystal size while maintaining or improving diffraction quality.

3.1.2. Crystal seeding. Another commonly used method for growing larger crystals is seeding, in which a crystal is transferred into a fresh protein/precipitant solution (Thaller *et al.*, 1981; Bergfors, 2003). We have experimented with this technique, transferring high-quality single crystals from 4 µl hanging drops (Fig. 2*a*) to either 25 µl of protein/precipitant solution or 25 µl of protein solution only in glass crystallization plates. Although no reservoir solution was present and the wells were sealed, protein and precipitant concentrations within these large sitting drops increased over time as the drops equilibrated with the enclosed space.

While crystals transferred to protein/precipitant solution continued their growth, crystals added to protein-only solution dissolved in the unsaturated solution as expected. Interestingly, new crystals appeared in this condition after several days, and these new crystals grew to a much larger final size than those transferred into the batch solution. Examples of the crystals obtained from the two seeding approaches are shown in Fig. 4.

Further seeding experiments involved transplanting crystals grown by hanging-drop vapour diffusion into capillaries (0.5 mm, Glass No. 50; Hampton Research) to provide a more protected environment for the crystals to grow in (Fig. 5). Capillaries eliminate excessive vapour diffusion and emulate the dynamics within hanging drops; the vertical column of mother liquor provided by capillaries helps to simulate the 'depth' of hanging drops and promotes three-dimensional growth. While transplanted crystals did indeed grow within the batch solution-containing capillaries, this approach also highlighted that relocating and feeding an already established crystal results in an undesirable increase in mosaicity, as also evident by the growth defects that were clearly visible within the transplanted crystal.

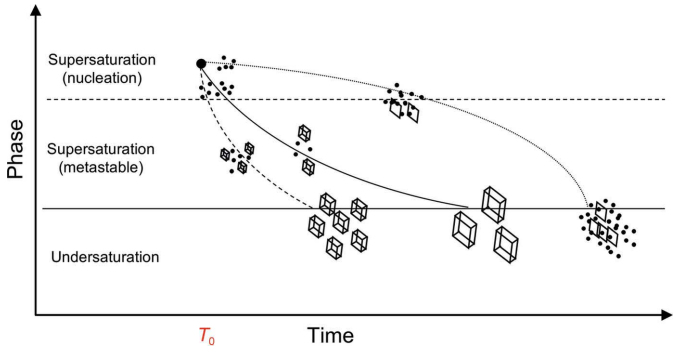

Figure 3
Crystal size is dependent on the phase–time pathway. Otherwise identical drops starting from the same point in phase space at time zero may produce significantly different outcomes depending on how the phase space changes over time. For example, a single drop (vapour-diffusion format) starting in the nucleation zone may result in numerous small crystals if the reservoir solution is too dilute, *i.e.* vapour diffusion proceeds at an insufficient rate to counteract the drive towards the solubility line as protein leaves solution as crystal or precipitate, and time spent in the growth phase is minimized. A more optimal reservoir composition results in fewer, larger crystals, as decreases in protein concentration over time are balanced by concurrent increases in precipitant concentration (owing to the equilibration of the drop with the reservoir), prolonging the time spent in the growth phase. Finally, a potent reservoir solution results in a large amount of protein precipitation and poorly developed crystals, as vapour diffusion provides a strong drive towards higher precipitant concentrations within the drop, and the time spent in the nucleation zone is extended.

Based on these findings, the most promising strategy for maximizing the size *and* the diffraction quality involves decoupling the nucleation and growth phases, as outlined in Supplementary Fig. S1. Allowing nucleation to occur naturally in a drop and keeping the developed nuclei within that drop as protein-rich solution is added means that the favourable environment around the nuclei is preserved locally and osmotic shock is prevented. In addition, it is also important that the mother liquor has a high concentration of protein and a low concentration of precipitant(s). This allows the drop to stay in the metastable region as the protein concentration decreases, which in turn enables extended crystal growth.

3.2. Crystallization within capillaries: counter-diffusion

Counter-diffusion (growing crystals in capillaries) offers a different approach to crystallization and possibly several advantages over vapour-diffusion methods when it comes to growing larger crystals for NMX (Ng *et al.*, 2003). Firstly, chaotic mixing and evaporation-driven convection are largely eliminated by the restrictive geometry of capillaries, providing a stabilized environment for crystal development. Secondly, the method is, to a certain degree, self-optimizing, with large areas of phase space explored within a single experiment (Otálora *et al.*, 2009). Thirdly, the setup is one-dimensional and hence is easily scalable by simply increasing the capillary diameter once crystallization conditions have been identified and the quest for large crystals starts.

We set up our counter-diffusion crystallization with solubilized SERCA1 along the length of the capillary, an agarose plug at the end of the capillary and the capillary itself immersed in crystallization buffer contained within a 1.5 ml Eppendorf tube. Initially, a supersaturation wave moves through the capillary, forming nuclei in a sporadic manner along the length of the capillary. Once this wave passes, the conditions stabilize and a supersaturation gradient, easing towards the distal end of the capillary, remains. The gradient produces a wide variety of local microenvironments across the mother liquor, and nuclei evolve into crystal polymorphs. Over time, the supersaturation gradient increases throughout the capillary as the precipitants continue to diffuse, driving crystal growth (see Supplementary Fig. S2).

Our initial results are promising, as can be seen in Fig. 6(*a*), although further optimization is clearly required. One issue is the inhibited diffusion of high-molecular-weight PEGs used as a crystallization agent across the 1% agarose plugs, as PEG diffusion through agarose reduces with increasing molecular weight and agarose concentration (Weng *et al.*, 2005). Trials with lower molecular-weight PEGs (PEG 400 and PEG 2000 as opposed to PEG 6000) and a reduced agarose concentration (0.5%) have so far not improved the crystallization

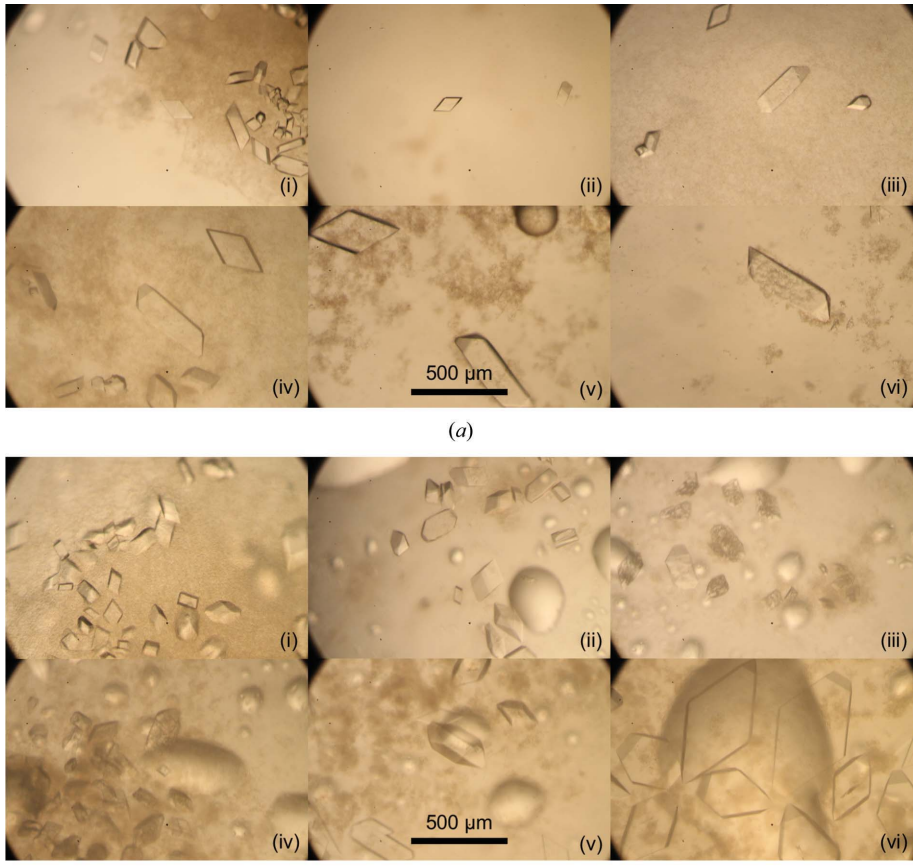

Figure 4
Seeding already established crystals. (*a*) Crystals grown in a 4 µl hanging drop (i) were transplanted into 25 µl batch solution (12.5 µl 14 mg ml^{-1} SERCA + 12.5 µl 9.33% PEG 6000, 8% glycerol) of equal composition (ii). Images of the transplanted crystals after 1, 3, 11 and 22 days show their evolution from continued growth (iii, iv) to maximum size (v) to deterioration (vi). (*b*) Crystals from a 4 µl hanging drop (i) were transplanted into 25 µl 14 mg ml^{-1} SERCA (ii). The crystals largely disintegrated after one day in the protein-rich solution (iii) and remained largely unchanged by day 3 (iv). Interestingly, new crystals that had appeared by day 11 (v) reached very large sizes by day 22 (vi).

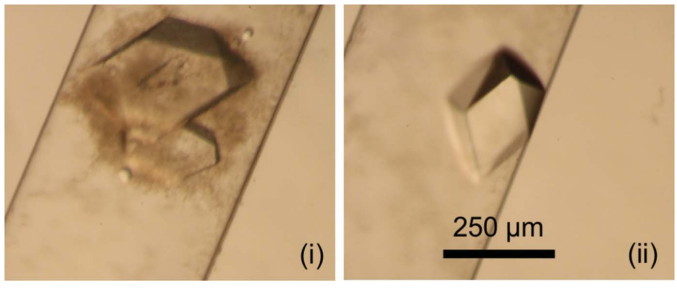

Figure 5
Comparison between a seeded and a native crystal. An established crystal (i) was placed within fresh batch solution inside a capillary to promote further growth compared with a crystal spontaneously arising from within the same batch solution alone (ii). Note that while the major transplanted crystal has achieved a larger size than the native crystal, stress fractures can be seen at its centre and its diffraction quality is compromised.

outcome. Another practical issue is the susceptibility of the agarose plug to become dislodged from the capillary, allowing chaotic mixing between the protein solution and the buffer. Moving forward, adding agarose directly to the protein solution to a final concentration of 0.1–0.3% agarose might address the issues that we have encountered so far.

In addition to the canonical setup described above, we explored a free-interface diffusion setup with solubilized SERCA carefully placed adjacent to crystallization buffer inside the capillary with no separating agarose barrier. This technique proved to be effective for quickly growing single crystals as the diffusion of precipitants is not restricted by agarose gel (Fig. 6*b*) and more closely follows the dynamics within hanging and sitting drops. Although the setup may not be useful for growing large crystals as the protein is stretched too thinly, the wide range of protein:precipitant ratios that it covers may prove to be useful for identifying crystallization conditions for further consideration.

4. Room-temperature X-ray diffraction

To test their diffraction potential, large crystals (approximately 200 × 150 × 100 µm) were analysed at room temperature (RT) using a laboratory home X-ray source. Although the source was far less powerful than synchrotron sources, the resulting data allowed us to assess RT X-ray diffraction characteristics, being indicative of how well neutrons will diffract under similar conditions. In addition, this test high-

Table 1
Summary of individual data sets.

Data sets 1–7 were indexed and integrated separately in *XDS*, before all `XDS_ASCII.HKL` files were scaled and merged into a single reflections file using the scaling module *aP_scale* (Vonrhein *et al.*, 2011). Phases were obtained by molecular replacement using *Phaser-MR* (McCoy *et al.*, 2007) with a refined Ca_2E1-AMPPCP structure (PDB entry 3n8g) as a search model. Model building was performed within *Coot* (Emsley *et al.*, 2010) and refinements were performed with *phenix.refine* (Afonine *et al.*, 2012).

	Unit-cell parameters							Resolution range† (Å)		
Crystal	*a* (Å)	*b* (Å)	*c* (Å)	*α* (°)	*β* (°)	*γ* (°)	Mosaicity (°)	Low	High	Wavelength (Cu *Kα*)
1	165.17	77.50	151.42	90.00	109.174	90.00	0.195	45.05	3.538	1.5418
2	165.68	77.44	152.31	90.00	109.241	90.00	0.168	45.05	3.790	1.5418
3	165.66	77.50	152.33	90.00	109.314	90.00	0.204	45.05	4.019	1.5418
4	165.47	77.30	151.75	90.00	109.296	90.00	0.235	45.05	4.222	1.5418
5	165.57	77.43	151.84	90.00	109.384	90.00	0.160	45.05	3.953	1.5418
6	165.54	77.41	151.76	90.00	109.312	90.00	0.127	45.05	3.711	1.5418
7	168.10	80.13	154.22	90.00	109.279	90.00	0.185	45.05	3.589	1.5418

† The resolution limit of each data set was determined by *aP_scale* according to the criteria that $R_{\rm p.i.m.} \leq 0.600$, $I/\sigma(I) \geq 1.00$ and $CC_{1/2} \geq 0.300$.

lighted some important aspects of the practical and technical challenges of isolating individual crystals within a sealed capillary (essential for performing neutron diffraction studies). An initial RT X-ray structure of the SERCA Ca_2E1-AMPPCP crystal form was solved.

4.1. Capillary mounting of crystals

Transferring a single crystal from a hanging or sitting drop into a capillary, removing the mother liquor surrounding it and then sealing the capillary at both ends without damaging the crystal proved to be extremely challenging. Once a crystal had finally been isolated and settled inside the capillary, some mother liquor was kept adjacent to the crystal, ideally on both sides, to maintain the vapour pressure inside the capillary to stabilize the crystal. The final challenge of sealing the capillary with wax also required great care.

The few crystals that managed to survive the process displayed poor diffraction owing to the stress of the mounting ordeal. This highlighted how fragile the SERCA crystals were,

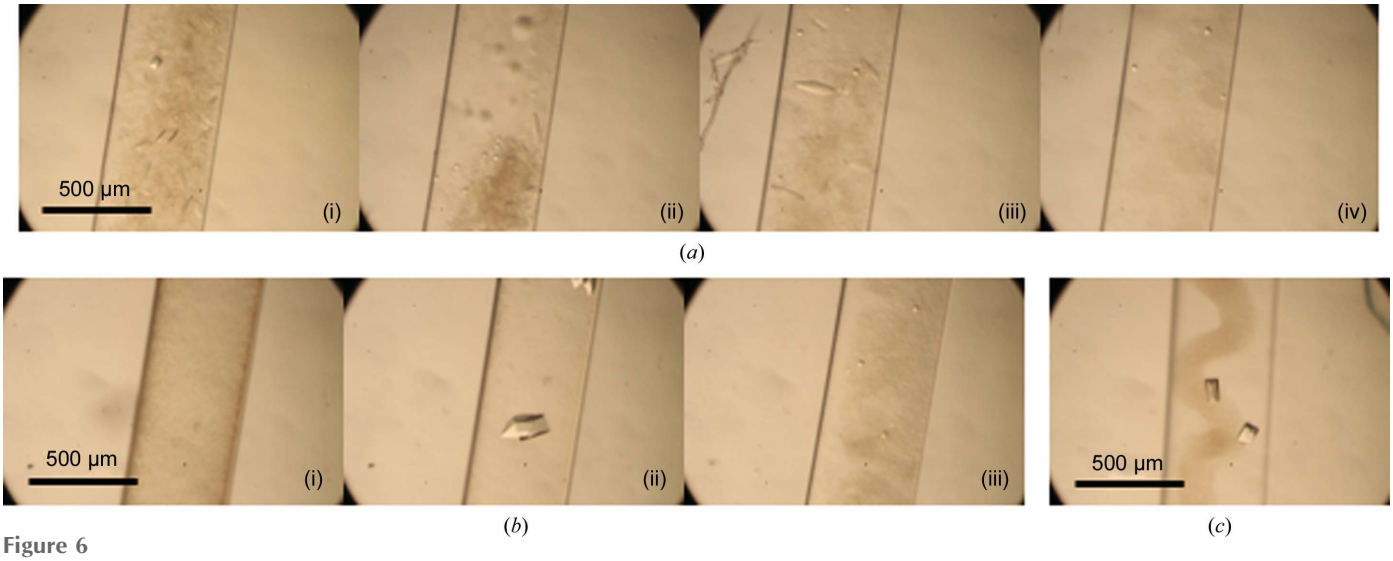

Figure 6
Counter-diffusion crystallization. (*a*) Images along the capillary are from nearest the protein–buffer interface (i) to most distant from the protein–buffer interface (iv). The capillary contained 15.9 mg ml^{-1} solubilized SERCA (plugged with ∼5 mm 1% agarose gel) and was immersed in crystallization buffer consisting of 12%(*w*/*w*) PEG 6000, 4%(*v*/*v*) *tert*-butanol, 14%(*v*/*v*) glycerol, 5 m*M* *β*-mercaptoethanol, 200 m*M* sodium acetate. A wide range of phase space is explored within this one capillary: largely uniform precipitate near the protein–buffer interface embedded with numerous two-dimensional crystals and two small crystals of good morphology (i), heterogeneous precipitation with clear, spheroidal globular bodies (ii), less dense, more homogeneous precipitation embedded with a few large two-dimensional crystals (iii) and almost fully solubilized solution with patches of light precipitation and a few clear, spheroidal globular bodies (iv). Images were taken three weeks after setting up. (*b*) Liquid–liquid free-interface crystallization within vertically orientated capillaries. Protein solution over crystallization buffer. Images along the capillary are from the bottom of the capillary (i) to the top (iii). The capillary contained 5 µl 16 mg ml^{-1} solubilized SERCA above a crystallization buffer consisting of 12%(*w*/*w*) PEG 6000, 4%(*v*/*v*) *tert*-butanol, 14%(*v*/*v*) glycerol, 5 m*M* *β*-mercaptoethanol, 200 m*M* sodium acetate. A variety of supersaturation environments exist within the capillary: protein-poor/precipitant-rich (i), protein-moderate/precipitant-moderate (ii) and protein-rich/precipitant-poor (iii). Images were taken three weeks after setting up. (*c*) Crystallization buffer over protein solution. The capillary contained 5 µl 16 mg ml^{-1} solubilized SERCA below a crystallization buffer consisting of 10.67%(*w*/*w*) PEG 6000, 4%(*v*/*v*) *tert*-butanol, 8%(*v*/*v*) glycerol, 5 m*M* *β*-mercaptoethanol, 200 m*M* sodium acetate. The less dense protein solution rises through the crystallization buffer, covering a wide range of protein:precipitant concentration ratios as it is drawn out. Single crystals occur at several points along the protein trail. The image was taken six days after setting up.

Table 2
Crystal data and structure refinement for the room-temperature structure (PDB entry 6hef).

Wavelength (Å)	1.5418
Resolution range (Å)	45–3.54 (3.67–3.54)
Space group	*C*2
Unit-cell parameters (Å, °)	a = 165.84, b = 77.77, c = 152.22, α = 90, β = 109.28, γ = 90
Total reflections	111920 (11439)
Unique reflections	22565 (1534)
Multiplicity	5.0 (5.1)
Completeness (%)	94.91 (68.47)
Mean $I/\sigma(I)$	4.63 (1.42)
Wilson B factor (Å^2)	85.1
R_{merge}	0.3055 (1.111)
R_{meas}	0.3433 (1.241)
$R_{p.i.m.}$	0.1529 (0.5416)
$CC_{1/2}$	0.933 (0.556)
CC*	0.983 (0.845)
Reflections used in refinement	21491 (1533)
Reflections used for R_{free}	1080 (84)
R_{work}	0.2228 (0.3169)
R_{free}	0.2595 (0.3443)
CC(work)	0.866 (0.769)
CC(free)	0.900 (0.493)
No. of non-H atoms	
Total	7760
Macromolecules	7671
Ligands	89
No. of protein residues	994
R.m.s.d., bonds (Å)	0.004
R.m.s.d., angles (°)	0.72
Ramachandran favoured (%)	94.7
Ramachandran allowed (%)	5.0
Ramachandran outliers (%)	0.3
Rotamer outliers (%)	0.00
Clashscore	9.28
Average B factor (Å^2)	
Overall	92.66
Macromolecules	92.65
Ligands	93.06
No. of TLS groups	8

and we focused on crystals grown directly inside the capillary, as outlined above, for X-ray diffraction. Crystals grown in this manner generally grew on the inner surface of the capillary and hence were already immobilized. Therefore, crystals could be isolated simply by removal of the liquid around them with a smaller capillary and reforming the immersion oil seal (Supplementary Fig. S3).

4.2. X-ray diffraction data collection

Sealed capillaries containing isolated crystals were mounted directly onto an AFC10/11 CCD single-crystal structure-analysis system (Rigaku, Tokyo, Japan) goniometer with modelling clay. Diffraction studies were performed at room temperature using a cryostream set to 293.15 K to ensure thermal stability. The maximum resolution seen in the analysed crystals was ∼3.0 Å (Supplementary Fig. S4), indicating that the SERCA Ca_2E1-AMPPCP form is suitable for neutron diffraction studies as, with further optimization, a resolution of 2.5–3 Å should be achievable at RT.

Another important result was the finding that this crystal form was highly susceptible to radiation damage at RT (Supplementary Fig. S5). This is worth keeping in mind, as one will ideally want to complement a neutron structure with an RT X-ray structure to ensure equivalency and to allow joint neutron/X-ray refinement (Afonine *et al.*, 2010).

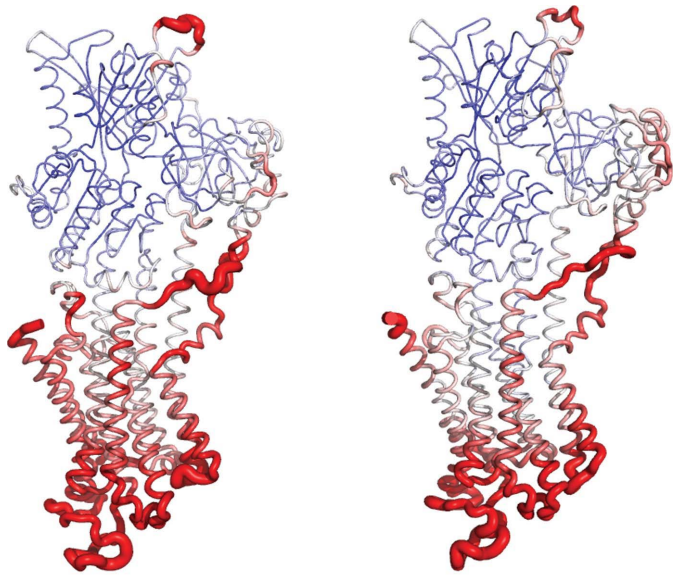

Figure 7
Comparison of (*a*) cryotemperature and (*b*) room-temperature structures of SERCA in the Ca_2E1-AMPPCP conformation. The structures are coloured according to B-factor value from 30 Å^2 (red) to 150 Å^2 (blue).

4.3. Room-temperature structure of SERCA1

Diffraction data were collected from nine crystals. Data from seven of these were scaled, merged and processed as summarized in Table 1. This combined data set was used for molecular replacement using PDB entry 3n8g as a search model. Final refinement statistics are summarized in Table 2.

The overall differences between the RT structure and the previously published structure collected at cryotemperature (100 K) are small; the r.m.s.d. is 1.575 Å over all atoms and 1.049 Å over main-chain atoms. Comparing the distance between each atom and the centre of mass for the two structures also shows a narrow and symmetric distribution, with only a slight positive shift, indicating that the two structures are similar with small variations and a minute temperature-dependent shift (Supplementary Fig. S6; Fischer *et al.*, 2015). The structures also show a comparable B-factor distribution, suggesting that the presence of calcium and the non-hydrolysable ATP analogue AMPPCP indeed induces a tight and well defined conformation that is stable at room temperature (Fig. 7).

5. Discussion

Here, we have demonstrated that it is possible to obtain large well diffracting crystals of SERCA that may be suitable for NMX. This was possible because (i) milligrams of protein are readily available from a natural source, (ii) we have well established purification and solubilization protocols in place

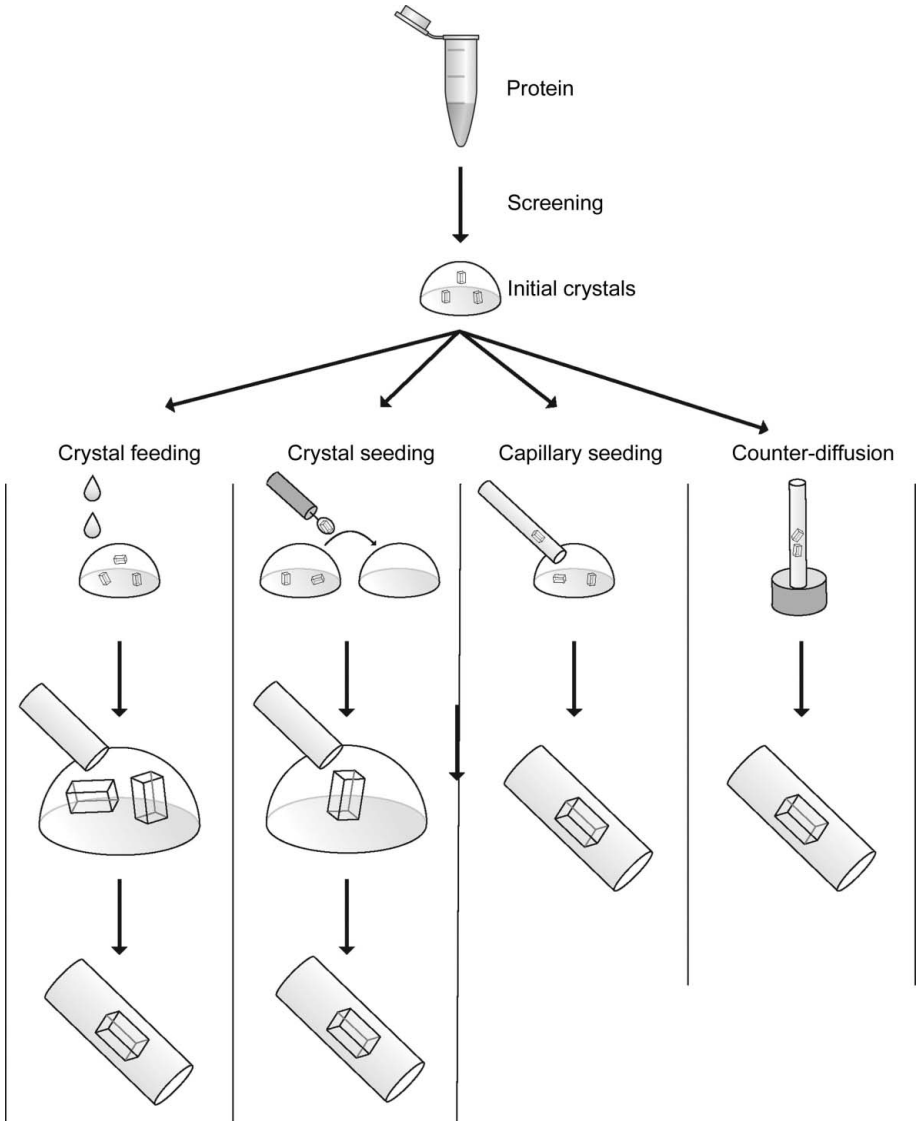

Figure 8
Overview of the workflow. Once initial crystallization conditions have been established, a number of paths are possible for increasing the crystal size. For crystal feeding and seeding the growing crystal is kept in a crystallization drop, with the final crystal being transferred to a capillary for data collection. For capillary seeding the growing crystal is transferred to a capillary. For counter-diffusion the crystal nucleates and grows in the capillary.

ensuring minimal batch variation and (iii) we have well characterized crystal forms with unit-cell parameters compatible with NMX data collection. We have established that after initial nucleation, several viable routes for obtaining large crystals of SERCA exist. These are summarized in the roadmap presented in Fig. 8. The finding that a large crystal will grow even when adding protein-only solution to initial crystal hits demonstrates that the metastable zone is very wide with respect to protein and precipitate concentrations in the case of SERCA. From a crystal-growth perspective, we are free to choose any of the available techniques. We currently favour growing crystals directly in capillaries, eliminating the mechanical stress caused when transferring large crystals from a drop to a capillary. This is a pragmatic decision that may change if other mounting procedures for extensive room-temperature data collection become easier.

Across all of the crystallization conditions tested, we always see precipitation in drops where we find nucleation. Batch crystallization has helped us to overcome this and has made the handling of crystals much easier. If, on the other hand, we reduce the protein and/or precipitant concentrations to avoid this initial precipitation, we do not see any nucleation. This suggests that the formation of propagative nucleation is rate-limiting and that we need to be well into the nucleation zone with many metastable clusters, and significant precipitation, in the crystallization drop for a successful nucleation event to take place (Vekilov, 2010). Alternatively, what we observe may be that a fraction of the protein is more susceptible to precipitation.

We also do not find any significant differences between the RT structure presented here and the previously published cryotemperature structures. This is in agreement with the

findings from a previously reported RT structure collected using a free-electron laser (Bublitz *et al.*, 2015). The positive shift of the peak seen in Supplementary Fig. S6 is small and confirms a very limited and uniform temperature effect between RT and cryotemperature structures.

When crystallizing membrane proteins, one is crystallizing a mixture of protein, lipids and detergent depending on the exact experimental conditions. As the function of SERCA is affected by the presence of specific phospholipids (Lee, 2003), we were anticipating that SERCA crystallization could be selective for specific lipids and hence result in the accumulation of unfavourable lipids in the crystal-growth phase, which in turn would render the crystal surface 'poisoned', inhibiting further crystal growth. Here, we have demonstrated the growth of large SERCA crystals; hence, a possible poisoning effect does not appear to have any significant effect on crystal growth.

It is essential to select the right crystal form for NMX and this should be considered during initial screening. The recent development of *in situ* screening facilities at synchrotrons provides a useful tool enabling a thorough sampling of the unit-cell parameters, symmetry and resolution of any initial hits to fully explore crystallization space (Grimes *et al.*, 2018).

Every protein target represents a unique crystallization challenge, and our findings with SERCA described here should serve as a guide to approaches that can tackle some of the challenges of crystallizing membrane proteins for NMX.

6. Related literature

The following references are cited in the Supporting Information for this article: Clausen *et al.* (2016), Czyzewski & Wang (2012), Fischer *et al.* (2009), Guo *et al.* (2015), Javelle *et al.* (2008), Kellosalo *et al.* (2012), Koepke *et al.* (2007, 2009), Laulumaa *et al.* (2015), Lanyi & Schobert (2007), Laursen *et al.* (2009), Malinauskaite *et al.* (2014), Møllerud *et al.* (2017), Moncoq *et al.* (2007), Norimatsu *et al.* (2017), Pflüger *et al.* (2018), Takahashi *et al.* (2007), Toyoshima *et al.* (2007, 2011), Wang *et al.* (2017) and Yamashita *et al.* (2005).

Acknowledgements

The authors would like to thank Anne Lillevang for expert technical assistance and Jonathan Juhl for preparing Supplementary Fig. S5.

References

Afonine, P. V., Grosse-Kunstleve, R. W., Echols, N., Headd, J. J., Moriarty, N. W., Mustyakimov, M., Terwilliger, T. C., Urzhumtsev, A., Zwart, P. H. & Adams, P. D. (2012). *Acta Cryst.* D**68**, 352–367.
Afonine, P. V., Mustyakimov, M., Grosse-Kunstleve, R. W., Moriarty, N. W., Langan, P. & Adams, P. D. (2010). *Acta Cryst.* D**66**, 1153–1163.
Bergfors, T. (2003). *J. Struct. Biol.* **142**, 66–76.
Bergfors, T. (2007). *Methods Mol. Biol.* **363**, 131–151.
Blakeley, M. P., Hasnain, S. S. & Antonyuk, S. V. (2015). *IUCrJ*, **2**, 464–474.
Blakeley, M. P., Langan, P., Niimura, N. & Podjarny, A. (2008). *Curr. Opin. Struct. Biol.* **18**, 593–600.
Bublitz, M., Musgaard, M., Poulsen, H., Thøgersen, L., Olesen, C., Schiøtt, B., Morth, J. P., Møller, J. V. & Nissen, P. (2013). *J. Biol. Chem.* **288**, 10759–10765.
Bublitz, M., Nass, K., Drachmann, N. D., Markvardsen, A. J., Gutmann, M. J., Barends, T. R. M., Mattle, D., Shoeman, R. L., Doak, R. B., Boutet, S., Messerschmidt, M., Seibert, M. M., Williams, G. J., Foucar, L., Reinhard, L., Sitsel, O., Gregersen, J. L., Clausen, J. D., Boesen, T., Gotfryd, K., Wang, K.-T., Olesen, C., Møller, J. V., Nissen, P. & Schlichting, I. (2015). *IUCrJ*, **2**, 409–420.
Buch-Pedersen, M. J., Pedersen, B. P., Veierskov, B., Nissen, P. & Palmgren, M. G. (2009). *Pflugers Arch.* **457**, 573–579.
Clausen, J. D., Bublitz, M., Arnou, B., Olesen, C., Andersen, J. P., Møller, J. V. & Nissen, P. (2016). *Structure*, **24**, 617–623.
Czyzewski, B. K. & Wang, D.-N. (2012). *Nature (London)*, **483**, 494–497.
Emsley, P., Lohkamp, B., Scott, W. G. & Cowtan, K. (2010). *Acta Cryst.* D**66**, 486–501.
Espinoza-Fonseca, L. M. (2017). *Mol. Biosyst.* **13**, 633–637.
Fischer, G., Kosinska-Eriksson, U., Aponte-Santamaría, C., Palmgren, M., Geijer, C., Hedfalk, K., Hohmann, S., de Groot, B. L., Neutze, R. & Lindkvist-Petersson, K. (2009). *PLoS Biol.* **7**, e1000130.
Fischer, M., Shoichet, B. K. & Fraser, J. S. (2015). *Chembiochem*, **16**, 1560–1564.
Gavira, J. A. (2016). *Arch. Biochem. Biophys.* **602**, 3–11.
Gerlits, O., Keen, D. A., Blakeley, M. P., Louis, J. M., Weber, I. T. & Kovalevsky, A. (2017). *J. Med. Chem.* **60**, 2018–2025.
Gourdon, P., Andersen, J. L., Hein, K. L., Bublitz, M., Pedersen, B. P., Liu, X.-Y., Yatime, L., Nyblom, M., Nielsen, T. T., Olesen, C., Møller, J. V., Nissen, P. & Morth, J. P. (2011). *Cryst. Growth Des.* **11**, 2098–2106.
Grimes, J. M., Hall, D. R., Ashton, A. W., Evans, G., Owen, R. L., Wagner, A., McAuley, K. E., von Delft, F., Orville, A. M., Sorensen, T., Walsh, M. A., Ginn, H. M. & Stuart, D. I. (2018). *Acta Cryst.* D**74**, 152–166.
Guo, Y., Kalathur, R. C., Liu, Q., Kloss, B., Bruni, R., Ginter, C., Kloppmann, E., Rost, B. & Hendrickson, W. A. (2015). *Science*, **347**, 551–555.
Jaeger, K., Dworkowski, F., Nogly, P., Milne, C., Wang, M. & Standfuss, J. (2016). *Adv. Exp. Med. Biol.* **922**, 137–149.
Javelle, A., Lupo, D., Ripoche, P., Fulford, T., Merrick, M. & Winkler, F. K. (2008). *Proc. Natl Acad. Sci. USA*, **105**, 5040–5045.
Jensen, A. M., Sørensen, T. L., Olesen, C., Møller, J. V. & Nissen, P. (2006). *EMBO J.* **25**, 2305–2314.
Kang, H. J., Lee, C. & Drew, D. (2013). *Int. J. Biochem. Cell Biol.* **45**, 636–644.
Kellosalo, J., Kajander, T., Kogan, K., Pokharel, K. & Goldman, A. (2012). *Science*, **337**, 473–476.
Koepke, J., Krammer, E. M., Klingen, A. R., Sebban, P., Ullmann, G. M. & Fritzsch, G. (2007). *J. Mol. Biol.* **371**, 396–409.
Koepke, J., Olkhova, E., Angerer, H., Müller, H., Peng, G. & Michel, H. (2009). *Biochim. Biophys. Acta*, **1787**, 635–645.
Lanyi, J. K. & Schobert, B. (2007). *J. Mol. Biol.* **365**, 1379–1392.
Laulumaa, S., Blakeley, M. P., Raasakka, A., Moulin, M., Härtlein, M. & Kursula, P. (2015). *Acta Cryst.* F**71**, 1391–1395.
Laursen, M., Bublitz, M., Moncoq, K., Olesen, C., Møller, J. V., Young, H. S., Nissen, P. & Morth, J. P. (2009). *J. Biol. Chem.* **284**, 13513–13518.
Lee, A. G. (2003). *Biochim. Biophys. Acta*, **1612**, 1–40.
Malinauskaite, L., Quick, M., Reinhard, L., Lyons, J. A., Yano, H., Javitch, J. A. & Nissen, P. (2014). *Nature Struct. Mol. Biol.* **21**, 1006–1012.
Manzoni, F., Saraboji, K., Sprenger, J., Kumar, R., Noresson, A.-L., Nilsson, U. J., Leffler, H., Fisher, S. Z., Schrader, T. E., Ostermann, A., Coates, L., Blakeley, M. P., Oksanen, E. & Logan, D. T. (2016). *Acta Cryst.* D**72**, 1194–1202.
McCoy, A. J., Grosse-Kunstleve, R. W., Adams, P. D., Winn, M. D., Storoni, L. C. & Read, R. J. (2007). *J. Appl. Cryst.* **40**, 658–674.

McPherson, A. (2017). *Methods Mol. Biol.* **1607**, 17–50.
Møller, J. V., Lenoir, G., Marchand, C., Montigny, C., le Maire, M., Toyoshima, C., Juul, B. S. & Champeil, P. (2002). *J. Biol. Chem.* **277**, 38647–38659.
Møller, J. V., Olesen, C., Winther, A. M. & Nissen, P. (2010). *Q. Rev. Biophys.* **43**, 501–566.
Møllerud, S., Pinto, A., Marconi, L., Frydenvang, K., Thorsen, T. S., Laulumaa, S., Venskutonytė, R., Winther, S., Moral, A. M. C., Tamborini, L., Conti, P., Pickering, D. S. & Kastrup, J. S. (2017). *ACS Chem. Neurosci.* **8**, 2056–2064.
Moncoq, K., Trieber, C. A. & Young, H. S. (2007). *J. Biol. Chem.* **282**, 9748–9757.
Moraes, I., Evans, G., Sanchez-Weatherby, J., Newstead, S. & Stewart, P. D. (2014). *Biochim. Biophys. Acta*, **1838**, 78–87.
Newstead, S. (2015). *Biochim. Biophys. Acta*, **1850**, 488–499.
Ng, J. D., Gavira, J. A. & García-Ruíz, J. M. (2003). *J. Struct. Biol.* **142**, 218–231.
Norimatsu, Y., Hasegawa, K., Shimizu, N. & Toyoshima, C. (2017). *Nature (London)*, **545**, 193–198.
O'Dell, W. B., Bodenheimer, A. M. & Meilleur, F. (2016). *Arch. Biochem. Biophys.* **602**, 48–60.
Oksanen, E., Chen, J. C.-H. & Fisher, S. Z. (2017). *Molecules*, **22**, 596.
Olesen, C., Picard, M., Winther, A. M., Gyrup, C., Morth, J. P., Oxvig, C., Møller, J. V. & Nissen, P. (2007). *Nature (London)*, **450**, 1036–1042.
Olesen, C., Sørensen, T. L., Nielsen, R. C., Møller, J. V. & Nissen, P. (2004). *Science*, **306**, 2251–2255.
Otálora, F., Gavira, J. A., Ng, J. D. & García-Ruiz, J. M. (2009). *Prog. Biophys. Mol. Biol.* **101**, 26–37.
Pflüger, T., Hernández, C. F., Lewe, P., Frank, F., Mertens, H., Svergun, D., Baumstark, M. W., Lunin, V. Y., Jetten, M. S. M. & Andrade, S. L. A. (2018). *Nature Commun.* **9**, 164.
Sakai, H., Fujii, T. & Takeguchi, N. (2016). *Met. Ions Life Sci.* **16**, 459–483.
Sørensen, T. L. & Andersen, J. P. (2000). *J. Biol. Chem.* **275**, 28954–28961.
Sørensen, T. L., Møller, J. V. & Nissen, P. (2004). *Science*, **304**, 1672–1675.
Sørensen, T. L., Olesen, C., Jensen, A. M., Møller, J. V. & Nissen, P. (2006). *J. Biotechnol.* **124**, 704–716.
Takahashi, M., Kondou, Y. & Toyoshima, C. (2007). *Proc. Natl Acad. Sci. USA*, **104**, 5800–5805.
Thaller, C., Weaver, L. H., Eichele, G., Wilson, E., Karlsson, R. & Jansonius, J. N. (1981). *J. Mol. Biol.* **147**, 465–469.
Toyoshima, C. & Mizutani, T. (2004). *Nature (London)*, **430**, 529–535.
Toyoshima, C. & Nomura, H. (2002). *Nature (London)*, **418**, 605–611.
Toyoshima, C., Nomura, H. & Tsuda, T. (2004). *Nature (London)*, **432**, 361–368.
Toyoshima, C., Norimatsu, Y., Iwasawa, S., Tsuda, T. & Ogawa, H. (2007). *Proc. Natl Acad. Sci. USA*, **104**, 19831–19836.
Toyoshima, C., Yonekura, S., Tsueda, J. & Iwasawa, S. (2011). *Proc. Natl Acad. Sci. USA*, **108**, 1833–1838.
Vekilov, P. G. (2010). *Cryst. Growth Des.* **10**, 5007–5019.
Vonrhein, C., Flensburg, C., Keller, P., Sharff, A., Smart, O., Paciorek, W., Womack, T. & Bricogne, G. (2011). *Acta Cryst.* D**67**, 293–302.
Walker, J. E. (2013). *Biochem. Soc. Trans.* **41**, 1–16.
Wang, S., Wacker, D., Levit, A., Che, T., Betz, R. M., McCorvy, J. D., Venkatakrishnan, A. J., Huang, X. P., Dror, R. O., Shoichet, B. K. & Roth, B. L. (2017). *Science*, **358**, 381–386.
Weber, I. T., Waltman, M. J., Mustyakimov, M., Blakeley, M. P., Keen, D. A., Ghosh, A. K., Langan, P. & Kovalevsky, A. Y. (2013). *J. Med. Chem.* **56**, 5631–5635.
Weng, L., Liang, S., Zhang, L., Zhang, X. & Xu, J. (2005). *Macromolecules*, **38**, 5236–5242.
Yamashita, A., Singh, S. K., Kawate, T., Jin, Y. & Gouaux, E. (2005). *Nature (London)*, **437**, 215–223.